



Tidal triggering of earthquakes suggests poroelastic behavior on the San Andreas Fault



Andrew A. Delorey^{a,*}, Nicholas J. van der Elst^b, Paul A. Johnson^a

^a Los Alamos National Laboratory, Geophysics Group, Mailstop D446, Los Alamos, NM 87544, United States

^b U.S. Geological Survey, Earthquake Science Center, 525 South Wilson Avenue, Pasadena, CA 91106, United States

ARTICLE INFO

Article history:

Received 24 August 2016

Received in revised form 9 December 2016

Accepted 10 December 2016

Available online 28 December 2016

Editor: P. Shearer

Keywords:

seismology
earthquake triggering
California
Earth tides
pore pressure

ABSTRACT

Tidal triggering of earthquakes is hypothesized to provide quantitative information regarding the fault's stress state, poroelastic properties, and may be significant for our understanding of seismic hazard. To date, studies of regional or global earthquake catalogs have had only modest successes in identifying tidal triggering. We posit that the smallest events that may provide additional evidence of triggering go unidentified and thus we developed a technique to improve the identification of very small magnitude events. We identify events applying a method known as inter-station seismic coherence where we prioritize detection and discrimination over characterization. Here we show tidal triggering of earthquakes on the San Andreas Fault. We find the complex interaction of semi-diurnal and fortnightly tidal periods exposes both stress threshold and critical state behavior. Our findings reveal earthquake nucleation processes and pore pressure conditions – properties of faults that are difficult to measure, yet extremely important for characterizing earthquake physics and seismic hazards.

© 2016 Elsevier B.V. All rights reserved.

1. Background

Earthquake triggering can occur in response to both quasi-static stress changes and dynamic forcing. Aftershocks are a well-known example of triggering by quasi-static and dynamic stress transfer, while triggering of distant earthquakes by seismic waves is an example of strictly dynamic triggering (Delorey et al., 2015; Gombert et al., 2004; Gonzalez-Huizar et al., 2012; Hill et al., 1993). Earthquake triggering has the potential to be extremely valuable in probing stress state characteristics such as critical state (near failure) conditions (Brinkman et al., 2015; Brodsky and van der Elst, 2014; Johnson et al., 2013; van der Elst et al., 2013). Triggering by Earth tides can be particularly informative since tides are always present and observations can be stacked in time, in contrast to dynamic earthquake triggering which can occur only during or after the passage of large amplitude seismic waves.

Earth tides are caused by the gravitational pull of the sun and moon, which induce periodic stresses related to the rotation of the Earth relative to the sun and moon (semi-diurnal, ~12 h and diurnal, ~24 h). A longer-period modulation of these cycles arises due to the orbit of the moon around the Earth (fortnightly, ~14.7 days). Earth tides impart both normal and shear stresses on

fault surfaces in the upper crust. During tidal-induced periods of increasing Coulomb stress on a fault, the stressing rate is much higher than the long-term tectonic stressing rate determined from the average stressing rate between M_w6 earthquakes near Parkfield, California (Agnew, 1997; Kim and Dreger, 2008). Tidal triggering of earthquakes has been observed locally preceding large earthquakes (Tanaka, 2010, 2012; Tanaka et al., 2002b), and also in global or regional datasets that span longer periods of time (Cochran et al., 2004; Metivier et al., 2009; Tanaka et al., 2002a; Tsuruoka et al., 1995). Tides also trigger earthquakes at volcanoes (Emter, 1997; McNutt and Beavan, 1981; Rydelek et al., 1988) and ocean tides (Stroup et al., 2007; Tolstoy et al., 2002; Wilcock, 2001, 2009) may trigger earthquakes in ocean basins.

Continental crust is thought to be critically stressed (Townend and Zoback, 2000) meaning that faults near failure are ubiquitous. If this is true, then we might expect earthquake triggering to be widespread in response to transient stresses associated with tides and large amplitude seismic waves; however this is not observed (Vidale et al., 1998). We propose that observations of the tidal triggering of earthquakes are scarce because most earthquakes and therefore most triggered earthquakes are small and below detection limits. The barrier to observing tidally triggered earthquakes may simply be a lack of completeness in the catalog. Thus our intent here is to improve detections of small earthquakes to determine if tidal triggering of earthquakes is occurring in regions where it is currently not detected using existing earthquake cat-

* Corresponding author.

E-mail addresses: andrew.delorey@lanl.gov (A.A. Delorey), nvanderelst@usgs.gov (N.J. van der Elst), paj@lanl.gov (P.A. Johnson).

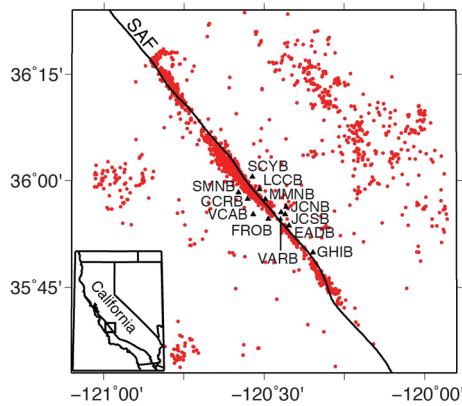


Fig. 1. Map. Red circles represent earthquakes from the NCSN catalog in calendar years 2012–2014 that are within 50 km of Parkfield, California and 50 km of the SAF. The black curve labeled “SAF” represents the San Andreas Fault. The labeled black triangles represent the stations of the HRSN used in this study. (For interpretation of the references to color in this figure, the reader is referred to the web version of this article.)

alogs. Our test case is a segment of the SAF near Parkfield, California (Fig. 1) because it is well instrumented, has a relatively high ambient seismicity rate, and is known to exhibit tidal triggering of low frequency earthquakes (LFEs) (Thomas et al., 2012; van der Elst et al., 2016) and non-volcanic tremors (NVTs) (Thomas et al., 2009) in the middle crust.

2. Earthquake catalogs

Traditional earthquake catalogs like that provided by the Northern California Seismic Network (NCSN) require a sufficient number of phase arrivals in order to estimate location and magnitude, which limits their completeness. Tidal correlation is suggested, but not statistically significant in the NCSN catalog (Fig. S1). We hypothesize that its significance could be limited by the stringency of the catalog location requirements. Thus, we develop a catalog in which we emphasize only detection and discrimination of phase arrivals so that the occurrence of smaller events may be cataloged, even when a precise location cannot be obtained (see examples in Figs. 2 and S2). Discrimination in this context means discriminating local, regular earthquakes from distant earthquakes, non-earthquake sources on Earth’s surface, and deeper LFEs and NVTs. We search for earthquakes by looking for seismic energy arriving across the NCSN that is consistent with emissions from local earthquakes.

NVTs are detected by identifying similar, emergent, long-duration waveforms across a seismic array cannot be explained by surface sources or noise (Obara, 2002). Correlation techniques are often used to identify and locate NVTs because they do not have impulsive or easily identifiable phase arrivals (Wech and Creager, 2008). Small earthquakes are similar in the sense that it is difficult to pick phase arrivals when the signal to noise ratio is low even when a signal has obvious earthquake characteristics. These earthquakes are missing from traditional catalogs because though they are often easily identified, they are difficult to characterize. Even with minimal characterization, these earthquakes contain valuable information and are worth cataloging.

We apply a similar approach to finding small earthquakes as others have used to find NVTs (Obara, 2002; Wech and Creager, 2008). We use unique array characteristics of local earthquakes to identify them in continuous data. Cross-correlating the waveform envelope, we look for energy within the 5–10 Hz band that has apparent velocities consistent with body waves emanating from sources within the local crust. Waves from regional and distant sources are highly attenuated in this band. The highest amplitude

waves from non-earthquake, surface sources have apparent velocities of surface waves and in the 5–10 Hz band have very small displacements at the depths of the borehole instruments of the NCSN. Also, since we do not use station pairs closer together than 5 km, only very energetic non-earthquake sources will be recorded on two or more instruments. (See methods for a full description of the earthquake detection method and the supplementary data for our complete catalog.)

Our coherence-derived earthquake catalog covers the calendar years 2012–2014 and contains 6735 earthquakes. In addition to the earthquakes we detect, we add 206 earthquakes from the NCSN catalog that are within 50 km of Parkfield and 5 km of the SAF that do not correspond to an earthquake in our base catalog, resulting in a total catalog of 6941 earthquakes. During the same period of time there are 1654 earthquakes in the NCSN earthquake catalog within 50 km of Parkfield and 5 km of the SAF. We do not determine a location for our detections other than to note the closest station. However by comparing our detections to matching detections in the NCSN earthquake catalog, we estimate that most (>90%) are also within about 50 km of Parkfield. 75% of the events in the NCSN catalog within 50 km of Parkfield are within 5 km of the SAF (Fig. S3), and thus we assume the same for our catalog. Our detections with matching entries in the NCSN earthquake catalog are not biased with regard to the distribution of depths found in the full NCSN catalog for the study period and region, which have a mean depth of 6.4 km and a median depth of 5.2 km.

For each earthquake in our catalog, we assign a phase for both the semi-diurnal cycle and the fortnightly cycle (Fig. S4). An important point is that the total tidal stress time series is not a simple sinusoid. When we refer to the semi-diurnal phase, what we mean is the phase associated with the total tidal stress time series, whose period is dominated by the semi-diurnal period of ~ 12.4 h. In any given cycle, the apparent period and phase is perturbed somewhat by the influence of other tidal components whose periods are close to 12 or 24 h. However, over long periods of time the average period is the semi-diurnal period. We determine the phase from the entire tidal stress time series because faults do not feel each tidal component independently. In the case of the fortnightly cycle, we use the timing of lunar phases to determine the phase.

We here consider temporal processes that could mimic tidally modulated clustering but be only coincidentally correlated with tidal stresses. The lunar semi-diurnal component (M_2) has the largest amplitude with more than twice that of the solar semi-diurnal component (S_2). The phase of the M_2 component dominates the phase of the total stress signal. With a period of ~ 12.4 h, the phase of the M_2 component progressively shifts relative to daytime and nighttime hours, so over the three year study period there is no net correlation with any diurnal signal anthropogenic or otherwise (see supplemental material). Potential biases introduced by seasonal processes do not affect the total catalog because the duration of our study is three full calendar years.

The other manner in which there may be apparent correlation of seismicity with tides is if aftershocks or other clustered events are correlated with tidal stresses but not caused by tidal stresses. Since our detection catalog contains only the timing of earthquakes, we do not have enough information to apply standard algorithms to remove aftershocks. Instead, we test the possibility that aftershock clustering could invalidate our measurements by creating 10000 synthetic catalogs that contain aftershocks using an ETAS model consistent with California seismicity (Field et al., 2014) but no explicit periodic forcing. We performed a maximum likelihood estimation (MLE) testing the periodicity of the synthetic catalogs against the periodicity of our catalog. Only 24 of the 10000 synthetic catalogs were more periodic than ours on the semi-diurnal cycle. All of these 24 synthetic catalogs contained

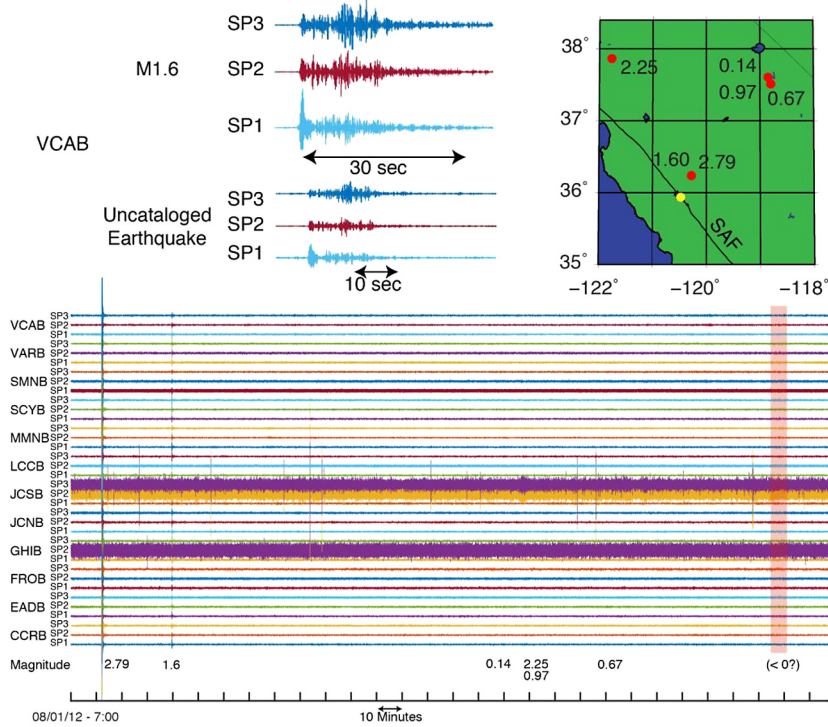


Fig. 2. Example of detected earthquake not present in the NCSN catalog. Shown are six earthquakes with magnitudes of 2.79, 1.60, 0.14, 2.25, 0.97, and 0.67 that are found in the NCSN catalog with an additional uncataloged earthquake found using our method. At upper left is a zoom of the traces from station VCAB with 5 Hz highpass filter and relative amplitudes preserved. The uncataloged earthquake whose magnitude is likely < 0 has similar waveforms to the cataloged M1.6 earthquake. At upper right are the locations of the six cataloged earthquakes (red circles) shown on the SAF. Some earthquakes are nearly co-located. Using our method, we detect events (red circles) on or near the SAF near Parkfield (yellow circle), but not those farther away (magnitudes 2.25, 0.14, 0.97, and 0.67). At bottom are traces from stations and components indicated at left with high pass filter at 1 Hz. The uncataloged event is shaded red, which is buried in the noise at this pass band. The closest cataloged LFE to this uncataloged regular earthquake is 16 minutes prior to it at 11:22:19. (For interpretation of the colors in this figure, the reader is referred to the web version of this article.)

a large ($M > 6.8$) earthquake whose aftershocks dominate the catalog statistics. No catalog with a maximum magnitude less than 6.8 was more periodic than ours. The maximum magnitude earthquake during our study period is 4.5.

Lastly, we examine how the observed correlation between seismicity and Earth tides varies over time and whether or not some short-duration behavior of the catalog dominates the statistics of the entire catalog. We determined that the observed correlation between Earth tides and seismicity is prevalent throughout the study period. Details of this analysis are in the supplemental materials.

3. Earth tides

Tidally induced strains can be modeled (Agnew, 1997) and with appropriate elastic moduli we can calculate stress at seismogenic depths allowing us to quantify the relationship between stress forcing (changes in Coulomb stress) and earthquake clustering. In the most general case, Skempton's coefficient (B) is a tensor, which measures how much of the normal stress is supported by pore pressures versus the rock matrix. However, we can consider more specific cases for an undrained fault system. Change in Coulomb stress (Beeler et al., 2000) for an anisotropic system and isotropic system, is respectively,

$$\Delta C = \Delta \tau + \mu(1 - B)\Delta \sigma \quad (1)$$

$$\Delta C = \Delta \tau + \mu(\Delta \sigma - B\Delta \sigma_m), \quad (2)$$

where ΔC is the change in Coulomb stress, $\Delta \tau$ is change in shear stress, μ is the coefficient of friction, $\Delta \sigma$ is the change in stress normal to the fault and $\Delta \sigma_m$ is the mean change in compressive stress. Positive σ is extensional. (A full description of tidal stress calculations can be found in the methods.)

4. Results

In order to characterize the observed clustering behavior in our catalog we first divide the lunar cycle into halves corresponding to rising and falling fortnightly tides. For events in these two halves we assign a phase value to each earthquake corresponding to its position in the semi-diurnal cycle. Our null hypothesis is that earthquake times correspond to a homogeneous Poisson distribution. We test the hypothesis that earthquakes times are periodic with the same periods as the semi-diurnal and fortnightly cycles and model the periodicity as a nonhomogeneous Poisson process. We then perform a MLE for the parameters of a periodic model for seismicity during rising and falling fortnightly tides with the same period as the semi-diurnal cycle. Finally we perform a likelihood ratio test comparing the periodic (nonhomogeneous) model to the homogeneous model.

Strictly speaking our catalog event times do not have a Poisson distribution because in a Poisson distribution there is no dependence of one event on another and our catalog contains aftershocks, which are dependent events. This has an impact on the likelihood values and ratios we calculate. However, we demonstrated with synthetic catalogs that aftershock clustering does not coincidentally produce periodic behavior. So, higher likelihoods calculated for the nonhomogeneous, periodic models are entirely due to better fitting of the tidally driven periodicity.

For seismicity during rising fortnightly tides we cannot reject the null hypothesis that earthquake times correspond to a homogeneous Poisson distribution (Fig. 3a, S5a). There is no apparent correlation between seismicity and semi-diurnal stress during rising fortnightly tides. Such a correlation either does not exist or is beyond our ability to detect it. However, for seismicity during falling fortnightly tides we reject the null hypothesis with a

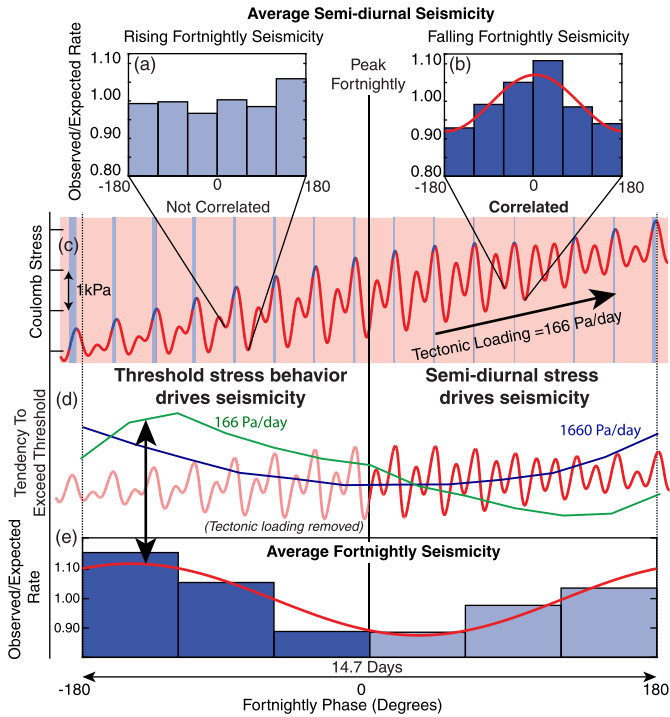


Fig. 3. Observations. Average seismicity as a function of semi-diurnal phase is shown during rising (a) and falling (b) fortnightly tides. Black sub-vertical lines connected to (c) indicate one semi-diurnal cycle (12.4 h). During rising fortnightly tides (a) seismicity is not correlated and during falling fortnightly tides (b) seismicity is correlated with the semi-diurnal stress cycle whose maximums are at phase zero. The red curve is the maximum likelihood periodic function for seismicity as a function of semi-diurnal phase. (c) Tidally driven Coulomb stress (effective $\mu = 0.5$) plus tectonic loading on SAF. Light blue regions indicate periods where stress threshold is exceeded while pink regions indicate periods of stress shadowing. (d) Green curve is tendency to exceed stress threshold as a function of fortnightly phase assuming a tectonic loading rate of 1660 Pa/day. Blue curve is tendency to exceed stress threshold as a function of fortnightly phase assuming a tectonic loading rate of 166 Pa/day. Red curve is tidally driven Coulomb stress on SAF without tectonic loading. During rising fortnightly tides threshold behavior drives seismicity (green solid curve); during falling fortnightly tides semi-diurnal stress drives seismicity (green dashed curve). (e) Average fortnightly seismicity for falling (blue) and falling (light blue) phase. Red curve is the maximum likelihood periodic function for seismicity as a function of fortnightly phase. (For interpretation of the colors in this figure, the reader is referred to the web version of this article.)

confidence of 0.986 (Fig. 3b, S5b). We also test the periodicity of all earthquakes with respect to the fortnightly cycle in the same manner, ignoring the semi-diurnal phase. We reject the null hypothesis with a confidence of 0.999 (Fig. 3e, S5c). We find that during falling fortnightly tides, seismicity peaks around the highest Coulomb stresses (peak rate lags peak stress by 5 degrees) within the semi-diurnal tidal cycle. Over the fortnightly cycle, earthquakes are more likely to be found at the beginning of the cycle when absolute peak stress (APS, the highest stress attained up to a point in time) is exceeded most often. A full description of our statistical analysis is in the methods.

We use an effective coefficient of friction of 0.5 to produce Fig. 3 because it produces tidally driven Coulomb stress that is dominated by the normal component, although our results change little for effective coefficients of friction between 0.4 and 1. If the effective coefficient of friction is close to zero then the phase of Coulomb stress is essentially the same as the phase of tidal shear stress and peak seismicity is anti-correlated with peak Coulomb stress. For higher effective coefficients of friction, the phase of Coulomb stress is the same as the phase of tidal normal stress and peak seismicity is positively correlated with peak Coulomb stress.

That the seismicity is correlated with tidal normal stress allows us to place constraints on frictional conditions on the SAF, namely

that the contribution of normal stress to the change in Coulomb stress is sufficiently larger than the contribution of shear stress for anisotropic or isotropic conditions, respectively,

$$\mu(1 - B)\Delta\sigma \gg \Delta\tau \quad (3)$$

$$\mu(\Delta\sigma - B\Delta\sigma_m) \gg \Delta\tau \quad (4)$$

During periods of maximum tidal shear stress $\Delta\tau \sim 220$ Pa and during periods of maximum tidal normal stress $\Delta\sigma \sim 2600$ Pa, $\Delta\sigma_m \sim 600$ Pa. If additionally the effective coefficient of friction is at least 0.4 then for anisotropic and isotropic conditions, respectively,

$$\mu(1 - B) \geq 0.4 \quad (5)$$

$$\mu \left(1 - B \frac{\Delta\sigma_m}{\Delta\sigma} \right) \geq 0.4 \quad (6)$$

To reiterate, we observe two apparently interdependent behaviors: 1) During rising tides, overall seismicity rates are high and earthquakes occur uniformly with respect to the semi-diurnal cycle; 2) During falling fortnightly tides, seismicity rates are lower, and earthquakes preferentially coincide with the peak semi-diurnal stress. To interpret the relationship between solid earth tides and seismicity we require a model that explains both behaviors. We look to observations and laboratory experiments for guidance in understanding the physical processes in the Earth.

5. Discussion and conclusions

Experiments and models generally define only narrow conditions in which tidal triggering of earthquakes should be detectable (Bartlow et al., 2012; Beeler and Lockner, 2003; Dieterich, 1987). Two important characteristics of tidal stresses at Parkfield have not been sufficiently explored: (1) tidal stresses are not simple sinusoids and (2) there is likely considerable stress shadowing—periods of time when stresses are below APS. The amount of stress shadowing depends heavily on the background or “tectonic” stressing rate, which can be estimated by the stress drops, afterslip, and inter-event times of large earthquakes (Murray and Langbein, 2006). To determine the average background stressing rate on the SAF near Parkfield we use the average stress drop of the 2004 Parkfield earthquake (Kim and Dreger, 2008) and divide it by the time interval since the previous large earthquake in 1966 to obtain a value of 166 Pa/day. We also consider higher loading rates due to stress concentrations. When combining tectonic and tidal stress two different kinds of stress shadows are produced, the shadow cast by peak semi-diurnal stress over subsequent semi-diurnal cycles, and the shadow cast by the peak of the fortnightly cycle on subsequent semi-diurnal cycles (Fig. 3c, 3d). The stress shadowing is so significant that APS is only exceeded $\sim 8\%$ of the time for a background loading rate of 166 Pa/day, and $\sim 25\%$ of the time for a background loading rate of 1660 Pa/day. These times are not evenly distributed over the semi-diurnal or fortnightly cycles (Fig. 3d).

If earthquakes only occur when APS is exceeded then they would only occur during the periods of blue in Fig. 3c and that is not what is observed. Additionally, periods of peak stressing rate are always in a stress shadow so it seems unlikely that peak seismicity should correlate with those times even though that is what is predicted for a purely threshold process (Beeler and Lockner, 2003). Stress shadows have been discussed but not fully explored for their affect on seismicity (e.g. Bartlow et al., 2012 and Thomas et al., 2012). For instance Bartlow et al. (2012) use a simple sinusoid to represent tidal stress and a background-stressing rate such that there are no stress shadows in their experiments. Thus, their results may not be representative of behavior on the SAF at Parkfield.

Rather than propose a new model, we discuss the role of stress shadows and the correlation between stress and seismicity in the context of rate and state friction (Dieterich, 2007) and stress threshold behavior. Existing models make specific predictions regarding stress and poroelastic conditions based on a system's response to periodic stressing (Bartlow et al., 2012; Beeler and Lockner, 2003; Dieterich, 1987; Thomas et al., 2012, 2009; van der Elst et al., 2016). Even without proposing a new model we can put some constraints on effective normal stress and poroelastic behavior, two important but often-inaccessible properties of a fault.

We consider that the observed difference in semi-diurnal tidal triggering between the rising and falling parts of the fortnightly cycle is related to the presence and distribution of stress shadows (Fig. 3). APS is exceeded most commonly during rising fortnightly tides (Fig. 3d), with long periods of stress shadowing more prevalent during falling fortnightly tides. During some fortnightly cycles, there can be multiple consecutive semi-diurnal cycles that do not emerge from within the stress shadow of the previous fortnightly peak stress (Fig. 3c). Seismicity rates overall are 10% higher during the phases of the fortnightly cycle in which the APS is most frequently exceeded (Fig. 3d, 3e). However, the correlation between seismicity and peak semi-diurnal stress is only evident during the waning fortnightly cycle, when APS is exceeded less often, and overall seismicity rates are lower (Fig. 3b, 3d). The effect of more frequently exceeding APS appears to be the dominant driver of the overall seismicity rate, which is secondarily driven by the semi-diurnal tides (Fig. 3d).

The sensitivity of seismicity to APS can be considered in terms of 'memory' of previous stress states. Many different materials, including Earth materials, exhibit a memory of past stress conditions. The Kaiser Effect (Kaiser, 1959; Kurita and Fujii, 1979) is a stress threshold effect where intact rock is fractured only when APS has been exceeded, which is manifest in elevated levels of acoustic emissions (AE), or earthquakes. Using the rate and state model of Beeler and Lockner (2003), shear resistance is the combined effect of shear resistance to slip and shear resistance necessary to break unfractured rock. The ratio of fractured to unfractured cross-sectional area is modeled as proportional to total slip. However, if the breaking of unfractured rock only or preferentially occurs when APS is exceeded, then either slip is suppressed when stress is below APS or the assumption of a linear relationship between total slip and area of fractured material is incorrect. When loading is uniform, the system is always exceeding APS rather than only during short time intervals so intact rock is always being fractured. According to the rate and state equations, during a period of rapid fracturing of rock, the associated fault weakening reduces the time-to-failure and the sensitivity of time-to-failure on stress variations. If there is a Kaiser Effect, this could explain both the increase in seismicity and undetected sensitivity to semi-diurnal stress variations during rising fortnightly tides. Once nucleation is initiated on a fault, it is in a state of elevated stress-sensitive creep. Within a stress shadow, the only sites that fail are those already experiencing stress-driven creep even if weakening is muted. Peak seismicity at these sites should correlate with local peak stress even when the stress is below APS (Bartlow et al., 2012; Beeler and Lockner, 2003; Li and Nordlund, 1993; Li et al., 2010; Liu et al., 2010). This would explain why earthquakes are observed during all parts of the tidal cycles, but preferentially at higher stresses within stress shadows.

An important application of tidal triggering of earthquakes is as an indicator of pore pressure and frictional behavior (Fig. 3). LFEs near Parkfield (but 10–15 km deeper than the earthquakes studied here) are triggered during peak tidal shear stresses (Thomas et al., 2009), but show little sensitivity to much larger increases in extensional stress. This suggests that the ratio of tidal shear stress to

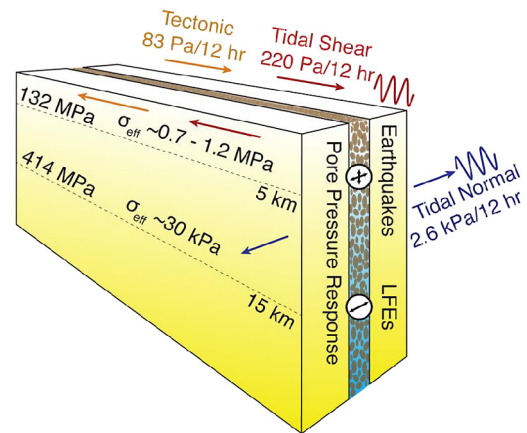


Fig. 4. Interpretation. The San Andreas Fault is loaded by tectonic shear stress (orange), tidal shear stress (red), and tidal normal stress (blue). Earthquakes in the upper crust are correlated with extensional tidal normal stress. Low frequency earthquakes in the middle crust are correlated with tidal shear stress. Lithostatic pressure, effective normal stress, and depth are indicated along dashed lines. In the middle crust, pore pressures respond to tidal normal stress with anisotropic poroelastic behavior, reducing the effective normal stress and canceling the contribution to Coulomb stress. In the upper crust poroelastic behavior is at least partially isotropic and normal stress contribution to Coulomb stress is only partially canceled. In short, tidal triggering of earthquakes transition from occurring during peak tidal extensional normal stresses to peak tidal shear stresses as pore pressures increase from below lithostatic pressure to near lithostatic pressure. (For interpretation of the colors in this figure, the reader is referred to the web version of this article.)

effective normal stress is high due to low effective normal stress resulting from near lithostatic pore pressure (see equation (1) in Thomas et al., 2012 and Dieterich, 2007),

$$R(\phi) = r \cdot \exp\left(\frac{C \cos \phi}{a\sigma}\right) \quad (7)$$

where ϕ is phase angle, R is seismicity rate, r is average seismicity rate, C is periodic Coulomb stress amplitude, a is the rate constitutive parameter (0.02) (Dieterich, 2007; Thomas et al., 2012), and σ is effective normal stress. The seismicity rate is sensitive to the effective normal stress and not to the ratio of shear to normal stress. An explanation for why LFEs show little sensitivity to much larger reductions in normal stress is that conditions are anisotropic and Skempton's coefficient is very close to one on the deep SAF (eq. (1)), which is common in low effective normal stress conditions (Beeler et al., 2013; Green and Wang, 1986; Hawthorne and Rubin, 2010; Houston, 2015). Any increase in extensional stress would be countered with an equal reduction in pore pressure resulting in no net change in effective normal stress or Coulomb stress (Fig. 4). Alternatively, very low μ could produce the same result.

We can estimate effective normal stress in the same way as Thomas et al. (2012) though in our case the result depends on Skempton's coefficient, B due to the interaction between tidal normal stresses and pore pressure. In the anisotropic case, $B < 0.6$ due to the constraint of equation (5), but this also requires μ to be higher than it is measured in the creeping section of the SAF to the north of Parkfield (Carpenter et al., 2015). B is rarely measured to be below 0.4 in Earth materials, e.g. Rice and Cleary (1976), leaving a small window where there are somewhat reasonable values for both μ and B . Using $B = 0.5$ and $\mu = 0.8$ with equation (1), the effective normal stress is 700 kPa, an order of magnitude higher than the 37 kPa determined for the middle crust in the vicinity of LFEs and tremor (Thomas et al., 2012). In the isotropic case B is not well constrained but has only a small effect on the results for effective normal stress which range from 1.2 MPa for $B = 0.5$ to 1.0 MPa for $B = 1$; both values are two orders of magnitude higher than that for the middle crust. As the stress drop for $M_w 6$ earth-

quakes on the SAF are at least 1 MPa, our preferred model is the isotropic one.

Pore pressure and effective normal stress are important parameters in frictional systems such as those in active tectonic regions as well as engineered environments associated with hydraulic fracturing, wastewater injection, and CO₂ sequestration. Based on results presented here, we posit that tidal triggering of earthquakes should transition from occurring during peak tidal extensional normal stresses to peak tidal shear stresses as pore pressures increase from below lithostatic pressure to near lithostatic pressure. If this were the case it could be highly useful in inferring time or space-dependent pore pressure and poroelastic behavior in both reservoir and tectonic environments.

The detection of tidal triggering is made possible by the interstation seismic coherence method, which focuses on earthquake detection at the expense of precise locations. This method offers a new and sensitive means to probe earthquake clustering behavior and the time-varying stress state of both tectonic and injection-activated faults.

Author contributions:

AD developed the earthquake detection method, performed the statistical analysis on the earthquake catalog, and contributed to the interpretation of the results. NVDE contributed to the statistical analysis of the earthquake catalog and the interpretation of the results. PAJ guided the direction of this study and contributed to the presentation and interpretation of the results. All authors participated in the writing of the manuscript.

Competing financial interests statement:

The authors have no competing interests.

Acknowledgements

Waveform data, metadata, or data products for this study were accessed through the Northern California Earthquake Data Center (NCEDC), <http://dx.doi.org/10.7932/NCEDC> and Southern California Earthquake Data Center (SCEDC) <http://dx.doi.org/10.7909/C3WD3xH1>. The LFE catalog is provided by David Shelly and is an update to the Shelly and Hardebeck (Shelly and Hardebeck, 2010) catalog. The authors wish to thank Earl Lawrence for consultations on statistical methods. AD and PJ received support from the U.S. Department of Energy (DOE) through the subTER Crosscut and institutional support from Los Alamos National Laboratory. NV received support from the Mendenhall postdoctoral program for this study.

Appendix A. Supplementary material

Supplementary material related to this article can be found online at <http://dx.doi.org/10.1016/j.epsl.2016.12.014>.

References

- Agnew, D.C., 1997. NLOADF: a program for computing ocean-tide loading. *J. Geophys. Res.* 102, 5109–5110. <http://dx.doi.org/10.1029/96jb03458>.
- Bartlow, N.M., et al., 2012. Laboratory triggering of stick-slip events by oscillatory loading in the presence of pore fluid with implications for physics of tectonic tremor. *J. Geophys. Res.* 117. <http://dx.doi.org/10.1029/2012jb009452>.
- Beeler, N.M., Lockner, D.A., 2003. Why earthquakes correlate weakly with the solid Earth tides: effects of periodic stress on the rate and probability of earthquake occurrence. *J. Geophys. Res.* 108. <http://dx.doi.org/10.1029/2001jb001518>.
- Beeler, N.M., et al., 2000. Pore fluid pressure, apparent friction, and Coulomb failure. *J. Geophys. Res.* 105, 25533–25542. <http://dx.doi.org/10.1029/2000jb900119>.
- Beeler, N.M., et al., 2013. Inferring fault rheology from low-frequency earthquakes on the San Andreas. *J. Geophys. Res.* 118, 5976–5990. <http://dx.doi.org/10.1002/2013jb010118>.
- Brinkman, B.A.W., et al., 2015. Probing failure susceptibilities of earthquake faults using small-quake tidal correlations. *Nat. Commun.* 6. <http://dx.doi.org/10.1038/ncomms7157>.
- Brodsky, E.E., van der Elst, N.J., 2014. The uses of dynamic earthquake triggering. *Annu. Rev. Earth Planet. Sci.* 42, 317–339. <http://dx.doi.org/10.1146/Annurev-Earth-060313-054648>.
- Carpenter, B.M., et al., 2015. Frictional properties of the active San Andreas Fault at SAFOD: implications for fault strength and slip behavior. *J. Geophys. Res.* 120, 5273–5289. <http://dx.doi.org/10.1002/2015jb011963>.
- Cochran, E.S., et al., 2004. Earth tides can trigger shallow thrust fault earthquakes. *Science* 306, 1164–1166. <http://dx.doi.org/10.1126/science.1103961>.
- Delorey, A.A., et al., 2015. Cascading elastic perturbation in Japan due to the 2012 Mw 8.6 Indian Ocean Earthquake. *Sci. Adv.* 1, e1500468. <http://dx.doi.org/10.1126/sciadv.1500468>.
- Dieterich, J.H., 1987. Nucleation and triggering of earthquake slip: effect of periodic stresses. *Tectonophysics* 144, 127–139. [http://dx.doi.org/10.1016/0040-1951\(87\)90012-6](http://dx.doi.org/10.1016/0040-1951(87)90012-6).
- Dieterich, J.H., 2007. *Applications of Rate- and State-Dependent Friction to Models of Fault Slip and Earthquake Occurrence*. Elsevier, New York.
- Emter, D., 1997. Tidal triggering of earthquakes and volcanic events. *Lect. Notes Earth Sci.* 66, 293–309.
- Field, E.H., et al., 2014. Uniform California earthquake rupture forecast, version 3 (UCERF3)—the time-independent model. *Bull. Seismol. Soc. Am.* 104, 1122–1180.
- Gomberg, J., et al., 2004. Earthquake nucleation by transient deformations caused by the $M = 7.9$ Denali, Alaska, earthquake. *Nature* 427, 621–624. <http://dx.doi.org/10.1038/Nature02335>.
- Gonzalez-Huizar, H., et al., 2012. Remote triggered seismicity caused by the 2011, M9.0 Tohoku-Oki, Japan earthquake. *Geophys. Res. Lett.* 39, L10302. <http://dx.doi.org/10.1029/2012GL051015>.
- Green, D.H., Wang, H.F., 1986. Fluid pressure response to undrained compression in saturated sedimentary-rock. *Geophysics* 51, 948–956. <http://dx.doi.org/10.1190/1.1442152>.
- Hawthorne, J.C., Rubin, A.M., 2010. Tidal modulation of slow slip in Cascadia. *J. Geophys. Res.* 115. <http://dx.doi.org/10.1029/2010jb007502>.
- Hill, D.P., et al., 1993. Seismicity remotely triggered by the magnitude 7.3 Landers, California, earthquake. *Science* 260, 1617–1623. <http://dx.doi.org/10.1126/Science.260.5114.1617>.
- Houston, H., 2015. Low friction and fault weakening revealed by rising sensitivity of tremor to tidal stress. *Nat. Geosci.* 8, 409–415. <http://dx.doi.org/10.1038/Ngeo2419>.
- Johnson, P.A., et al., 2013. Acoustic emission and microslip precursors to stick-slip failure in sheared granular material. *Geophys. Res. Lett.* 40, 5627–5631. <http://dx.doi.org/10.1002/2013gl057848>.
- Kaiser, E.J., 1959. A study of acoustic phenomena in tensile test, Technische Hochschule Munchen.
- Kim, A., Dreger, D.S., 2008. Rupture process of the 2004 Parkfield earthquake from near-fault seismic waveform and geodetic records. *J. Geophys. Res.* 113. <http://dx.doi.org/10.1029/2007jb005115>.
- Kurita, K., Fujii, N., 1979. Stress memory of crystalline rocks in acoustic-emission. *Geophys. Res. Lett.* 6, 9–12. <http://dx.doi.org/10.1029/GL006i001p00009>.
- Li, C., Nordlund, E., 1993. Experimental-verification of the Kaiser effect in rocks. *Rock Mech. Rock Eng.* 26, 333–351. <http://dx.doi.org/10.1007/BF01027116>.
- Li, Y.H., et al., 2010. Experimental and theoretical analysis on the procedure for estimating geo-stresses by the Kaiser effect. *Int. J. Miner. Metal. Mater.* 17, 514–518. <http://dx.doi.org/10.1007/s12613-010-0351-3>.
- Liu, J.P., et al., 2010. Experimental study on load/unload response ratio and Kaiser effect when rocks under cycling load. In: *Rock Stress and Earthquakes*, pp. 205–209.
- McNutt, S.R., Beavan, R.J., 1981. Volcanic earthquakes at Pavlof volcano correlated with the solid Earth tide. *Nature* 294, 615–618. <http://dx.doi.org/10.1038/294615a0>.
- Metivier, L., et al., 2009. Evidence of earthquake triggering by the solid Earth tides. *Earth Planet. Sci. Lett.* 278, 370–375. <http://dx.doi.org/10.1016/j.epsl.2008.12.024>.
- Murray, J., Langbein, J., 2006. Slip on the San Andreas fault at Parkfield, California, over two earthquake cycles, and the implications for seismic hazard. *Bull. Seismol. Soc. Am.* 96, S283–S303. <http://dx.doi.org/10.1785/0120050820>.
- Obara, K., 2002. Nonvolcanic deep tremor associated with subduction in southwest Japan. *Science* 296, 1679–1681. <http://dx.doi.org/10.1126/Science.1070378>.
- Rice, J.R., Cleary, M.P., 1976. Some basic stress diffusion solutions for fluid-saturated elastic porous-media with compressible constituents. *Rev. Geophys.* 14, 227–241. <http://dx.doi.org/10.1029/RG014i002p00227>.
- Rydelek, P.A., et al., 1988. Tidal triggering of earthquake swarms at Kilauea Volcano, Hawaii. *J. Geophys. Res.* 93, 4401–4411. <http://dx.doi.org/10.1029/JB093iB05p04401>.
- Shelly, D.R., Hardebeck, J.L., 2010. Precise tremor source locations and amplitude variations along the lower-crustal central San Andreas Fault. *Geophys. Res. Lett.* 37. <http://dx.doi.org/10.1029/2010gl043672>.
- Stroup, D.F., et al., 2007. Pulse of the seafloor: tidal triggering of microearthquakes at 9 degrees 50'N East Pacific Rise. *Geophys. Res. Lett.* 34. <http://dx.doi.org/10.1029/2007gl030088>.
- Tanaka, S., 2010. Tidal triggering of earthquakes precursory to the recent Sumatra megathrust earthquakes of 26 December 2004 (M-w 9.0), 28 March 2005

- (M-w 8.6), and 12 September 2007 (M-w 8.5). *Geophys. Res. Lett.* 37, L02301. <http://dx.doi.org/10.1029/2009gl041581>.
- Tanaka, S., 2012. Tidal triggering of earthquakes prior to the 2011 Tohoku-Oki earthquake (M-w 9.1). *Geophys. Res. Lett.* 39. <http://dx.doi.org/10.1029/2012gl051179>.
- Tanaka, S., et al., 2002a. Evidence for tidal triggering of earthquakes as revealed from statistical analysis of global data. *J. Geophys. Res.* 107. <http://dx.doi.org/10.1029/2001jb001577>.
- Tanaka, S., et al., 2002b. Spatio-temporal variation of the tidal triggering effect on earthquake occurrence associated with the 1982 South Tonga earthquake of Mw 7.5. *Geophys. Res. Lett.* 29. <http://dx.doi.org/10.1029/2002gl015386>.
- Thomas, A.M., et al., 2012. Tidal triggering of low frequency earthquakes near Parkfield, California: implications for fault mechanics within the brittle-ductile transition. *J. Geophys. Res.* 117. <http://dx.doi.org/10.1029/2011jb009036>.
- Thomas, A.M., et al., 2009. Tremor-tide correlations and near-lithostatic pore pressure on the deep San Andreas fault. *Nature* 462, 1048–1051. <http://dx.doi.org/10.1038/Nature08654>.
- Tolstoy, M., et al., 2002. Breathing of the seafloor: tidal correlations of seismicity at Axial volcano. *Geology* 30, 503–506. [http://dx.doi.org/10.1130/0091-7613\(2002\)030<0503:Botstc>2.0.Co;2](http://dx.doi.org/10.1130/0091-7613(2002)030<0503:Botstc>2.0.Co;2).
- Townend, J., Zoback, M.D., 2000. How faulting keeps the crust strong. *Geology* 28, 399–402. [http://dx.doi.org/10.1130/0091-7613\(2000\)28<399:Hfkctcs>2.0.Co;2](http://dx.doi.org/10.1130/0091-7613(2000)28<399:Hfkctcs>2.0.Co;2).
- Tsuruoka, H., et al., 1995. Statistical test of the tidal triggering of earthquakes – contribution of the Ocean tide loading effect. *Geophys. J. Int.* 122, 183–194. <http://dx.doi.org/10.1111/j.1365-246X.1995.tb03546.x>.
- van der Elst, N.J., et al., 2016. Fortnightly modulation of San Andreas tremor and low-frequency earthquakes. *Proc. Natl. Acad. Sci.* 113, 8601–8605. <http://dx.doi.org/10.1073/pnas.1524316113>.
- van der Elst, N.J., et al., 2013. Enhanced remote earthquake triggering at fluid-injection sites in the midwestern United States. *Science* 341, 164–167. <http://dx.doi.org/10.1126/Science.1238948>.
- Vidale, J.E., et al., 1998. Absence of earthquake correlation with Earth tides: an indication of high preseismic fault stress rate. *J. Geophys. Res.* 103, 24567–24572. <http://dx.doi.org/10.1029/98jb00594>.
- Wech, A.G., Creager, K.C., 2008. Automated detection and location of Cascadia tremor. *Geophys. Res. Lett.* 35. <http://dx.doi.org/10.1029/2008gl035458>.
- Wilcock, W.S.D., 2001. Tidal triggering of micro earthquakes on the Juan de Fuca Ridge. *Geophys. Res. Lett.* 28, 3999–4002. <http://dx.doi.org/10.1029/2001gl013370>.
- Wilcock, W.S.D., 2009. Tidal triggering of earthquakes in the Northeast Pacific Ocean. *Geophys. J. Int.* 179, 1055–1070. <http://dx.doi.org/10.1111/j.1365-246x.2009.04319.x>.